

# Stellar population astrophysics (SPA) with the TNG<sup>★</sup>

## Revisiting the metallicity of Praesepe (M44)

V. D’Orazi<sup>1,2</sup>, E. Oliva<sup>3</sup>, A. Bragaglia<sup>4</sup>, A. Frasca<sup>5</sup>, N. Sanna<sup>3</sup>, K. Biazzo<sup>5</sup>, G. Casali<sup>3</sup>, S. Desidera<sup>1</sup>, S. Lucatello<sup>1</sup>, L. Magrini<sup>3</sup>, and L. Origlia<sup>4</sup>

<sup>1</sup> INAF Osservatorio Astronomico di Padova, vicolo dell’Osservatorio 5, I-35122 Padova, Italy  
e-mail: valentina.dorazi@inaf.it

<sup>2</sup> Monash Centre for Astrophysics, School of Physics and Astronomy, Monash University, Melbourne, VIC 3800, Australia

<sup>3</sup> INAF Osservatorio Astrofisico di Arcetri, Largo E. Fermi 5, I-50125 Firenze, Italy

<sup>4</sup> INAF Osservatorio di Astrofisica e Scienza dello Spazio di Bologna, via Gobetti 93/3, I-40129 Bologna, Italy

<sup>5</sup> INAF Osservatorio Astrofisico di Catania, via S. Sofia 78, I-95123 Catania, Italy

Received ; accepted

### ABSTRACT

**Context.** Open clusters exquisitely track the Galactic disc chemical properties and its time evolution: a substantial number of studies and large spectroscopic surveys focus [mostly] on the chemical content of relatively old clusters (age  $\gtrsim 1$  Gyr). Interestingly, the less-studied young counterpart populating the solar surrounding has been found to be solar (at most), with a notable, surprising lack of young metal-rich objects. While there is wide consensus about the moderately above-solar composition of the Hyades cluster, the metallicity of Praesepe is still controversial. Recent studies suggest these two clusters share identical chemical composition and age, but this conclusion is disputed.

**Aims.** With the aim of re-assessing the metallicity of Praesepe, and its difference (if any) with the Hyades cluster, we present in this paper a spectroscopic investigation of 10 solar type dwarf members.

**Methods.** We exploited *GIARPS* at the TNG to acquire high-resolution, high-quality optical and NIR spectra and derived stellar parameters, metallicity ([Fe/H]), light,  $\alpha$  and iron-peak elements, by using a strictly differential (line-by-line) approach. We also analysed in the very same way the solar spectrum and the Hyades solar analogue HD 28099.

**Results.** Our findings suggest that Praesepe is more metal-rich than the Hyades, at the level of  $\Delta[\text{Fe}/\text{H}] = +0.05 \pm 0.01$  dex, with a mean value of  $[\text{Fe}/\text{H}] = +0.21 \pm 0.01$  dex. All the other elements scale with iron, as expected. This result seems to reject the hypothesis of a common origin for these two open clusters. Most important, Praesepe is currently the most metal-rich, young open cluster living in the solar neighbourhood.

**Key words.** Stars: abundances – Stars: solar-type – (Galaxy:) open clusters and associations: individual: M44

## 1. Introduction

Open clusters (OCs) are nowadays extensively exploited as light-houses to brighten our comprehension of the Galactic disc properties (chemistry, kinematics, and dynamics) and their evolution with time. A conspicuous number of works in the literature have been committed to investigate a variety of issues, such as e.g., the radial metallicity gradient (e.g., Reddy et al. 2016; Magrini et al. 2017), the internal dispersion in cluster abundances as evidence for stellar mixing and evolutionary processes (e.g., Drazdauskas et al. 2016), and the environmental dependence [clusters *vs.* field] of planet formation and survival (e.g., Delgado Mena et al. 2018, Fujii & Hori 2019). It is not surprising that several large spectroscopic surveys have directed their research interests to open cluster science, covering a broad range in terms of ages,

Galactocentric distances and metallicity (e.g., the Gaia-ESO survey, Gilmore et al. 2012; APOGEE, Donor et al. 2018). The path towards a comprehensive understanding of the Galactic disc formation and (chemical) evolution is, however, still long and tortuous.

There is compelling evidence from past and current studies that intermediate-age and young OCs (we can globally group them in clusters with ages  $\lesssim 1$  Gyr) in the solar neighbourhood exhibit a solar or even sub-solar iron abundance (e.g., Viana Almeida et al. 2009; D’Orazi et al. 2011; Spina et al. 2017 and references therein). In all these previous studies, which targeted very young ( $\lesssim 100$  Myr) clusters and associations, typical (internal) errors range between 0.15 and 0.20 dex, because of the intrinsic difficulty in the analysis of young stars (accretion, rotation and chromospheric activities play an important role in this case). On the other hand, when slightly older OCs are chemically characterised, internal precision of less than  $\sim 0.05$  dex can be reached. The lack of young and metal-rich clusters is somehow at odds with what is expected from standard chemical evolution (e.g., Chiappini et al. 2003): an enrichment of  $[\text{Fe}/\text{H}] \approx 0.10 - 0.15$  dex is predicted for the solar neighbourhood in the last few 4/5 Gyrs (e.g., Minchev et al. 2013). The only cluster in the solar vicinity that appears to have a signif-

<sup>★</sup> Based on observations made with the Italian Telescopio Nazionale Galileo (TNG) operated on the island of La Palma by the Fundación Galileo Galilei of the INAF (Istituto Nazionale di Astrofisica) at the Spanish Observatorio del Roque de los Muchachos of the Instituto de Astrofísica de Canarias. This study is part of the Large Program titled SPA - Stellar Population Astrophysics: the detailed, age-resolved chemistry of the Milky Way disk (PI: L. Origlia), granted observing time with HARPS-N and GIANO-B echelle spectrographs at the TNG.

icant enhancement in its chemical content is the Hyades OC, with an age between  $650 \pm 70$  Myr (Martín et al. 2018) and  $750 \pm 100$  Myr (Brandt & Huang 2015). Previous studies agree with a mild over-solar metallicity, including  $[\text{Fe}/\text{H}] = +0.13 \pm 0.06$  (Heiter et al. 2014), and  $[\text{Fe}/\text{H}] = +0.146 \pm 0.004$  (Cummings et al. 2017), to name a few. As part of our project, we have analysed for the first time the chemical composition of the young Northern OC ASCC123 ( $\approx 100$ – $150$  Myr), by studying a sample mostly composed of fast rotators, with a purposely designed technique (Frasca et al. 2019). Our findings argue that this young cluster is definitely not more metal-poor than the Sun, with a slightly super-solar composition, i.e.  $[\text{Fe}/\text{H}] = +0.14 \pm 0.04$  dex. However, given the large(r) errors related to the analysis of fast-rotating stars, a direct comparison with slightly older OCs, for which genuine, (non rotating) solar analogues are analysed in a very homogeneous way, is not reliable.

Quite controversial is instead the metallicity of the Praesepe cluster (NGC 2632/M44), located at  $d = 185.5_{-3.3}^{+3.5}$  pc (the Gaia collaboration, Cantat-Gaudin et al. 2018) with age estimates ranging between a gyro-chronological value of  $578 \pm 12$  Myr by Delorme et al. (2011), and  $790 \pm 60$  Myr (Brandt & Huang 2015) [but see the recent work by Gossage et al. (2018) for contrasting results]. As for the metal content, Friel & Boesgaard (1992) found  $[\text{Fe}/\text{H}] = +0.04 \pm 0.04$ , based on six F dwarf stars, while An et al. (2007) analysed four G dwarfs and obtained  $[\text{Fe}/\text{H}] = +0.11 \pm 0.03$ . Pace et al. (2008) derived instead a super-solar metallicity from seven Praesepe dwarf stars, with an average value of  $[\text{Fe}/\text{H}] = +0.27 \pm 0.10$ . Conversely, five years later, Boesgaard et al. (2013) analysed 11 solar-type stars via high-resolution spectroscopy and found a mean metallicity of  $[\text{Fe}/\text{H}] = +0.12 \pm 0.04$ , in contrast to the super-metal rich nature inferred by Pace and collaborators, and in agreement with An et al. (2007). The conclusion by Boesgaard et al. (2013) has been later confirmed by Cummings et al. (2017), who analysed moderate-resolution WYIN/Hydra spectra ( $R \sim 15,000$ ) for dwarfs in the Hyades and the Praesepe. They concluded that both OCs share consistent values of age and metallicity.

With the aim of further investigating this discrepancy we report, in this work, metallicity and elemental abundances for a sample of 10 solar-type dwarfs in the Praesepe observed with GIARPS (GIANO-B + HARPS-N), at the Telescopio Nazionale Galileo (TNG). Along with a differential analysis with respect to the solar spectrum, acquired with the same instrument, we have also analysed (with the same approach) the Hyades member HD 28099, which is included also in the sample of Liu et al. (2016). To ascertain whether young, metal-rich OCs do exist in the solar vicinity is not a secondary-order issue for several reasons, which include, but are not limited to, the connection between metallicity and the frequency of gas-giant planets (e.g., Santos et al. 2004; Johnson et al. 2010 and references therein), the present chemical composition of the solar neighbourhood, and the Galactic chemical evolution at recent epochs. Interestingly, the Praesepe OC could represent the most metal-rich, young OC living in the solar surroundings. We describe in Sec. 2 the observational sample along with data reduction and analysis techniques, while we present in Sec. 3 our results and the comparison with previous estimates. The Section 4 ends this manuscript with some considerations and a short discussion.

## 2. Observations and Analysis

We used GIARPS (Claudi et al. 2016) at the 3.6m telescope TNG to target 10 solar-type dwarfs in the Praesepe (Table 1), selected from high-probability members ( $P = 0.9$ – $1$ ) as published

by Cantat-Gaudin et al. (2018). Observations were carried out between December 2018 and January 2019. The instrument configuration allows to operate with the HARPS-N spectrograph ( $R = 115000$ ,  $\lambda\lambda = 3800$  –  $6900$  Å, Cosentino et al. 2014), and the GIANO-B near-infrared (NIR) spectrograph ( $R = 50000$ ,  $0.97$ – $2.5$   $\mu\text{m}$ , Oliva et al. 2012a, 2012b; Origlia et al. 2014). The second fibre of HARPS-N was pointed on-sky, to avoid contamination from the calibration lamp. Typical exposure times range between 1800 and 5400 seconds, with signal-to-noise (S/N) ratio between 45 and 75 (per pixel) at  $\lambda = 6000$  Å. For star N2632-32 the three different exposures were combined together to improve the low S/N (less than 20 per exposure). HARPS-N spectra were reduced by the instrument Data Reduction Software pipeline.

For an optimal subtraction of the detector artefacts and background, the GIANO-B spectra were collected nodding the star along the slit; i.e. with the target alternatively positioned at 1/4 (position A) and 3/4 (position B) of the slit length. Exposure time was 5 minutes per A,B position. The nodding sequences were repeated to achieve the same integration time as HARPS-N. The spectra have been reduced using the offline version of the GOFIO reduction software (Rainer et al. 2018)<sup>1</sup>, while the telluric correction has been performed using the spectra of a telluric standard (O-type star) taken at different air masses. More details on the data reduction and telluric correction techniques can be found in Origlia et al. (2019).

The membership of our 10 stars to the cluster has been confirmed by their radial velocities (RVs), which have been measured using the task *rvidlines* in IRAF<sup>2</sup>, employing 180 spectral lines. The RV values for each star, listed in Table 1, lead to an average cluster  $\text{RV} = 34.5 \pm 0.3$  km s<sup>-1</sup> (standard deviation 1.1 km s<sup>-1</sup>).

Spectroscopic parameters ( $T_{\text{eff}}$ ,  $\log g$ , microturbulence velocity  $\xi$ ), and abundances of Na, Mg, Al, Si, Ca, Fe, Ti, and Ni have been obtained with equivalent width (EW) measurements, by using the optical spectra. The line list, covering the wavelength range 4000 – 6900 Å, is provided in Table A.2. We have adopted for iron and titanium  $\log g f$  values from laboratory measurements, while we have obtained astrophysical values -from reverse solar analysis- for lines of other species for which laboratory measurements are currently not available. In this case we have adopted the same line list employed in D’Orazi et al. (2017, see that paper for details). As for Fe I and Fe II we have 86 and 17 lines, respectively.

EWs have been measured using the *ARES* code (Sousa et al. 2007), with substantial manual intervention (with IRAF) especially for lines located in the blue part of the spectrum ( $\lambda < 5000$  Å), due to the intrinsic difficulties in optimal continuum tracing. EW measurements for all our sample stars are available through CDS (an excerpt from the table is shown in Table 2).

Abundance analysis has been carried out using MOOG by C. Sneden (1973; 2017 version) and the Castelli & Kurucz (2004) grid of model atmospheres, with solar-scaled chemical composition and new opacities (ODFNEW). In order to improve the S/N, HARPS-N spectra (nominal resolution  $R = 115000$ ) have been degraded to the resolution of  $R = 45000$ ; typical final values for S/N are around 120–150 (per pixel) at 6000 Å. This has been done for all our sample stars and the solar spectrum, because our analysis is strictly differential (i.e., line-by-line) with respect to the Sun. This is the reason why our sample comprises

<sup>1</sup> <https://atreides.tng.iac.es/monica.rainer/gofio/>

<sup>2</sup> IRAF is the Image Reduction and Analysis Facility, a general purpose software system for the reduction and analysis of astronomical data. IRAF is written and supported by National Optical Astronomy.

**Table 1.** Information for our sample solar-type stars. Coordinates and  $J$ ,  $H$ , and  $K$  magnitudes are from 2MASS (Skrutskie et al. 2006);  $G$  magnitudes from Gaia. Radial velocities (RVs) are from the present study.

star	alias	RA (J2000)	Dec (J2000)	$G$ (mag)	$J$ (mag)	$H$ (mag)	$K$ (mag)	RV (km s <sup>-1</sup> )
N2632-6	KW 466	08:42:32.25312	+19:23:46.3272	10.845	9.836	9.536	9.458	33.40±0.06
N2632-7	KW 335	08:40:48.32832	+19:55:18.9228	10.863	9.864	9.588	9.507	34.47±0.07
N2632-8	KW 432	08:41:55.87008	+19:41:22.9596	10.896	9.869	9.627	9.544	33.52±0.06
N2632-9	KW 301	08:40:27.43008	+19:16:40.9296	11.008	10.012	9.698	9.655	32.91±0.08
N2632-10	HIP 42106	08:34:59.63856	+21:05:49.2000	11.009	10.012	9.761	9.684	35.43±0.05
N2632-25	KW 196	08:39:35.53992	+18:52:36.7356	10.581	9.657	9.381	9.329	35.08±0.06
N2632-26	KW 541	08:37:33.07704	+18:39:15.6600	10.532	9.621	9.347	9.283	35.35±0.05
N2632-27	TYC-1387-851-1	08:30:55.46544	+19:33:19.7784	10.647	9.725	9.463	9.369	36.38±0.06
N2632-28	KW 309	08:40:31.69320	+19:51:01.0512	11.431	10.294	9.985	9.911	35.23±0.03
N2632-32	ANM 1903	08:49:06.70008	+19:41:11.3892	11.721	10.533	10.173	10.068	33.61±0.05

**Table 2.** EW measurements (in milli Angstroms) for our 10 sample stars for which HARPS-N spectra have been analysed. The complete table is available through CDS.

Line	Species	EW <sub>N6</sub>	EW <sub>N7</sub>	EW <sub>N8</sub>	EW <sub>N9</sub>	EW <sub>N10</sub>	EW <sub>N25</sub>	EW <sub>N26</sub>	EW <sub>N27</sub>	EW <sub>N28</sub>	EW <sub>N32</sub>
6154.23	11.0	39.8	49.1	49.4	52.0	48.2	43.5	40.3	49.0	60.4	71.0
6160.75	11.0	61.7	72.8	66.5	69.0	68.2	58.6	57.7	63.2	73.5	95.0
.....	.....	.....	.....	.....	.....	.....	.....	.....	.....	.....	.....

only solar-type dwarf stars, while giants are not included. The spectrum of Ganymede (S/N=700 per pixel at 6000 Å) was acquired with GIARPS in the framework of the GAPS program (Global Architecture of Planetary systems, Covino et al. 2013). Our solar analysis results in  $T_{\text{eff}}=5780\pm50\text{K}$ ,  $\log g = 4.44 \pm 0.10$  dex,  $\xi=0.95\pm0.10$  km s<sup>-1</sup>, and  $A(\text{Fe I})=7.48\pm0.01\pm0.05$ , and  $A(\text{Fe II})=7.47\pm0.02\pm0.04$  (errors are on EW measurements and stellar parameters, respectively). Solar abundances for other species are listed in Table 3, along with the values by Asplund et al. (2009). For Na we have applied non-LTE corrections, following the prescriptions by Lind et al. (2011). In addition to the solar spectrum, we have included in our analysis the Hyades solar analogue HD 28099, which was observed with GIARPS on August 2019 as part of our SPA program. The S/N per pixel at 6000 Å is 180, after degrading the spectral resolution to R=45,000 as for all our sample stars.

Initial  $T_{\text{eff}}$  have been assumed from average photometric  $T_{\text{eff}}$ , which were obtained from  $J - K$  and  $V - K$  colours (see Table 1) and the calibration by Casagrande et al. (2010), assuming  $[\text{Fe}/\text{H}]=+0.10$  dex for the transformations. As for reddening, we have adopted  $E(B - V)=0.027$  from Taylor (2006) that has been converted to  $E(V - K)$  and  $E(J - K)$  by using  $A_V=3.086\times E(B - V)$  and  $A_K=A_V\times0.114$ ,  $A_J=A_V\times0.282$  (Cardelli et al. 1989). The magnitudes  $J$  and  $K$  were retrieved from the 2MASS catalogue (Skrutskie et al. 2006), whereas  $V$  magnitudes were obtained by transforming Gaia  $G$  magnitudes, following Evans et al. (2018).

**Table 3.** Solar abundances from the present study (HARPS-N and GIANO-B spectra) along with values by Asplund et al. (2009). Errors include only EW uncertainties and the number of spectral features used in the analysis is reported between parentheses.

Species	HARPS-N	GIANO-B	Asplund+(2009)
Na I	6.22±0.01(2)	6.24±0.02(1)	6.24±0.04
Mg I	7.63±0.04(2)	7.59±0.01(6)	7.60±0.04
Al I	6.49±0.01(2)	6.45±0.01(2)	6.45±0.03
Si I	7.52±0.02(11)	7.56±0.02(4)	7.51±0.03
Ca I	6.33±0.03(9)	6.32±0.02(2)	6.34±0.04
Ti I	4.97±0.01(52)	4.93±0.01(1)	4.95±0.05
Fe I	7.48±0.01(86)	7.49±0.01(19)	7.50±0.04
Ni I	6.24±0.01(16)	6.24±0.02(2)	6.22±0.04

The agreement with final spectroscopic values is satisfactory, with a mean difference of  $13\pm15$  K; the comparison between the two different values is given in Fig. 1. Initial surface gravity of  $\log g=4.45$  dex and  $\xi=1.00$  km s<sup>-1</sup> have been adopted. Spectroscopic final parameters were then inferred following the standard approach:  $T_{\text{eff}}$  and  $\xi$  have been derived by minimising trends between abundances from Fe I lines and excitation potential (E.P.)

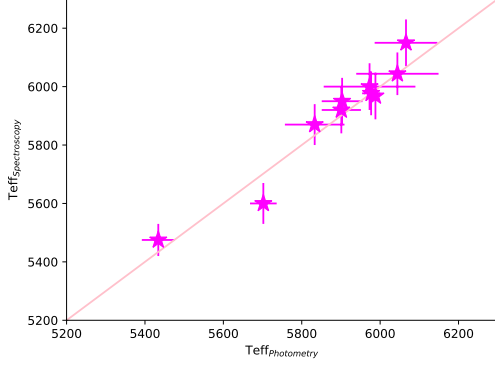


**Fig. 1.** Comparison between average photometric temperatures and our final spectroscopic values.

and reduced EWs, respectively. This is done by imposing that the slope of the correlations has to be within 1 sigma of its error. Surface gravities were determined from the ionisation equilibrium condition: the agreement between abundances from Fe I and Fe II lines has to be better than roughly one-third the scatter of their measurements (see Meléndez et al. 2014, D’Orazi et al. 2017). The errors in stellar parameters were computed from errors on the slopes for  $T_{\text{eff}}$  and  $\xi$ , while for  $\log g$  values the uncertainty estimate is given when the ionisation balance, as defined above, is no longer satisfied. The internal uncertainties on our derived abundances include errors due to EW measurements and to stellar parameters (calculating by varying one parameter at the time and inspecting the corresponding variation on the derived abundances; see Table 4). For further details on error computations we refer the reader to D’Orazi et al. (2017).

**Table 4.** Abundance sensitivities to change in stellar parameters for N2632-25 and N2632-32

Species	$\Delta T_{\text{eff}}$ (+100K)	$\Delta \log g$ (+0.2 dex)	$\Delta \xi$ (+0.2 km s <sup>-1</sup> )	$\Delta [A/H]$ (+0.2 dex)
N2632-25				
A(Na I)	+0.04	-0.01	-0.01	-0.01
A(Al I)	+0.04	-0.05	-0.03	0.00
A(Mg I)	+0.04	-0.01	-0.01	-0.01
A(Si I)	+0.02	-0.01	-0.02	+0.01
A(Ca I)	+0.05	-0.04	-0.04	-0.00
A(Ti I)	+0.08	-0.02	-0.03	-0.01
A(Ti II)	+0.00	+0.08	-0.06	+0.04
A(Fe I)	+0.06	-0.02	-0.05	0.00
A(Fe II)	-0.02	+0.07	-0.05	+0.04
A(Ni I)	+0.05	-0.02	-0.03	0.00
N2632-32				
A(Na I)	+0.06	-0.04	-0.03	0.00
A(Al I)	+0.06	-0.07	-0.03	+0.03
A(Mg I)	+0.05	-0.02	-0.02	0.00
A(Si I)	+0.00	+0.02	-0.02	+0.04
A(Ca I)	+0.07	-0.07	-0.04	+0.02
A(Ti I)	+0.11	-0.04	-0.05	0.00
A(Ti II)	+0.00	+0.07	-0.05	+0.08
A(Fe I)	+0.07	-0.03	-0.05	+0.03
A(Fe II)	-0.04	+0.10	-0.04	+0.08
A(Ni I)	+0.04	+0.00	-0.03	+0.04

Due to technical problems, most of the spectra were acquired with the telescope out of optimal focus. This had a much stronger effect on the NIR data because of the smaller aperture of GIANO (0.5 arcsec). Consequently, only for star N2632-6 we could achieve a sufficiently high S/N to perform a proper spectral analysis. Abundances from NIR spectral lines have been extracted via spectral synthesis calculations by using the driver *synth* in MOOG, and the same set of model atmospheres as derived from the optical spectra. An example of Fe I lines under scrutiny in this study are shown in Fig. 2 (see the Appendix for the line list with corresponding atomic parameters and references, Table A.1). Our approach consists in synthesising a region of 100 Å, including the line of interest, and varying in steps of 0.1 dex a given abundance: the best-fit is provided from the synthetic spectrum minimising the difference with the observed one (with a  $\chi^2$  test). The full line list used in the computations of the synthetic lines has been provided by C. Sneden (private communication). This has been done for the Sun and for the Praesepe star (we report in the Appendix Table A.1 line-by-line abundances for both cases, whereas average solar abundances from GIANO-B spectrum are listed in Col. 3 of Table 3).

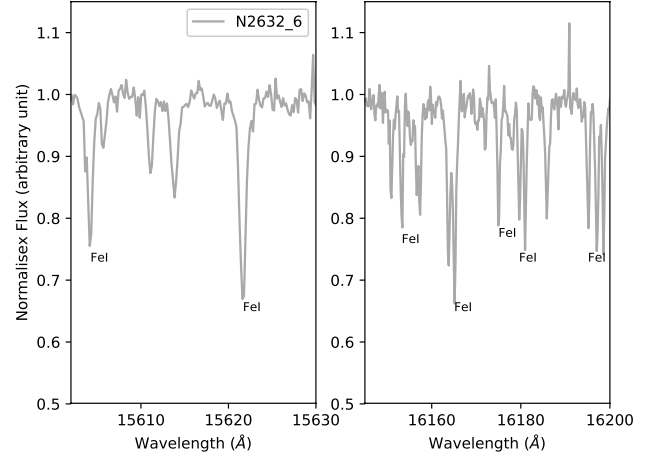


**Fig. 2.** Two segments of GIANO-B spectrum for star N2632-6. Seven out of the 19 Fe I lines in the H band that we used for abundance determination have been marked.

### 3. Results

Our results for stellar parameters and metallicity from HARPS-N spectra are shown in Table 5. From our sample we obtained an average cluster metallicity of  $[Fe/H]=+0.21\pm0.01$  (simple mean and standard error of the mean, with an internal dispersion of r.m.s.=0.02 dex), which is in contrast to Boesgaard et al. (2013) and Cummings et al. (2017). We searched for possible explanations of this discordance. First, we compared EW measurements for star KW 335 (N2632-7), which is the only star in common with Boesgaard et al. (2013) for which the authors made publicly available their EWs. For this star they obtained  $[Fe/H]=+0.13\pm0.04$  dex, that is 0.1 dex lower than our estimate. There is a small difference (based on 11 lines in common) of  $\Delta(EW)=2.2\pm5.3$  mÅ (see Fig. 3), and in  $\log gf$  values ( $\Delta \log gf=0.07\pm0.09$  dex), which alone cannot explain the  $[Fe/H]$  disagreement. Most important, we have differences of

+61 K in  $T_{\text{eff}}$ , +0.14 dex in  $\log g$ , and  $-0.06 \text{ km s}^{-1}$  in  $\xi$ , respectively. Had we instead adopted their stellar parameters, we would have inferred a  $[\text{Fe}/\text{H}] = +0.17$  dex, which is 0.06 dex lower than our determination but still larger than that of Boesgaard et al. (2013) of +0.04 dex. However, adopting their atmospheric parameters, the condition of excitation equilibrium (i.e., no trend between iron abundances and EP of the lines) is no longer satisfied, suggesting that the temperature they adopted is too cool (note that they used  $T_{\text{eff}}$  from the infra-red flux method and did not derive spectroscopic temperatures). To fully recover the difference between the two  $[\text{Fe}/\text{H}]$  estimates, a different solar composition with respect to ours might have been used by Boesgaard and collaborators, but their solar values are not published. We have three stars in common with Cummings et al. (2017), namely KW 466, KW 335, and KW 432 for which the authors derived  $[\text{Fe}/\text{H}] = +0.159^{+0.056}_{-0.067}$ ,  $[\text{Fe}/\text{H}] = +0.147^{+0.029}_{-0.031}$ , and  $[\text{Fe}/\text{H}] = +0.123^{+0.048}_{-0.054}$ , respectively. The comparison with our estimates indicates we have differences of +0.04, +0.08, and +0.15 dex for the three stars, while  $T_{\text{eff}}$  differ of +100K, +170K, and +279 K, respectively; this can explain the resulting discrepancy in  $[\text{Fe}/\text{H}]$ . It is noteworthy that their temperatures are not spectroscopically optimised, and were calculated assuming  $E(\text{B}-\text{V}) = 0.00$ , despite the fact it could be up to 0.03 mag (we have in fact adopted the value of  $E(\text{B}-\text{V}) = 0.027$  by Taylor 2006 in our photometric temperature calculations). The same authors concluded that there could be the possibility that Praesepe is slightly reddened, which would cause a higher  $[\text{Fe}/\text{H}] = +0.21$  dex (in agreement with our estimates) and a younger isochronal age (570 Myr), as also derived from gyro-chronology (Delorme et al. 2011). This, in turn, would discard the common origin hypothesis for Praesepe and Hyades (see Cummings et al. 2017). We cannot perform a star-by-star comparison for the other atmospheric parameters (i.e.,  $\log g$ , and  $\xi$ ) because these values are not published in the paper by Cummings et al. (2017); however we note, in passing, that also surface gravity and microturbulence values were adopted using photometry, that is from isochrones and the relationship by Edvardsson et al. (1993), respectively. Unfortunately, no stars are in common with Pace et al. (2008), who derived an even larger metallicity for the cluster members, but we refer to that paper for an extensive discussion about photometric vs. spectroscopic temperatures.

As for the other elements, we found that  $[\text{X}/\text{H}]$  ratios for Na, Mg, Al, Si, Ca, Ti I, Ti II, and Ni track iron, as expected. Star-by-star abundances for each species are listed in Table 6 (errors here are only those related to EWs, but see Table 4 for sensitivities to stellar parameters). The cluster mean values are reported in the last row (simple average and standard error of the mean). As a sanity check, to avoid the presence of spurious trends, we report in Fig. 4 the run of  $[\text{X}/\text{H}]$  ratios as a function of our derived  $T_{\text{eff}}$ . The analysis of the NIR spectra for star N2632-6 gives results in very good agreement with abundances from the optical spectrum (single-line abundances resulting from spectral synthesis calculations are given in Table A.1). We have mean differences of  $\Delta[\text{X}/\text{H}]_{(\text{NIR}-\text{OPT})} = +0.01, +0.05, +0.00, -0.05, +0.06, -0.03, +0.01$ , and  $+0.04$  dex for Na, Mg, Al, Si, Ca, Ti (only neutral lines), Fe, and Ni. The lack of systematic offsets in abundances between optical and NIR spectra (Fig. 4) for species under consideration here is also evident from the solar spectrum analysis, and corroborates previous results by Caffau et al. (2019), who reported a systematic investigation based on 40 stars (see that paper for details).

A careful inspection of the individual abundances for our sample stars (Tab. 5, and  $[\text{Fe}/\text{H}]$  plotted in Figure 4) reveals the presence of an outlier, characterised by a significant higher metal

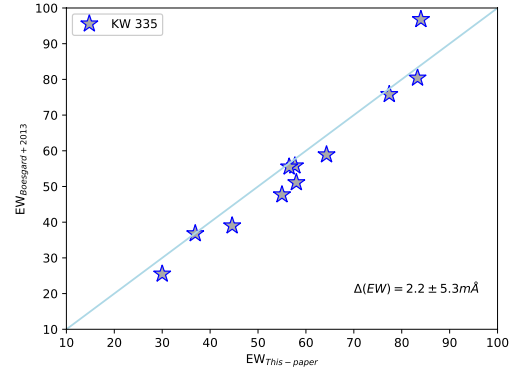


**Fig. 3.** Equivalent width comparison between our analysis and Boesgaard et al. (2013) for star KW 335.

content, that is star N2632-8, with  $[\text{Fe}/\text{H}] = +0.27 \pm 0.01$  dex. Although we might be dealing with a simple statistical fluctuation, we will investigate the nature of this significant enhancement, which is not due either to errors in  $T_{\text{eff}}$  or to a lower value of microturbulence velocity (see Tab. 5, by acquiring higher S/N spectra in the near future). Nevertheless, despite the lower quality of the present dataset for this kind of investigation, we have detected a preliminary indication of a positive trend between the condensation temperature of the species (including C measurements from two high-excitation C I lines) and differential abundances of this star with respect to the other cluster members with similar  $T_{\text{eff}}$ . The possible correlation with planetary formation or engulfment episodes is intriguing and certainly deserves further investigations.

#### 4. Discussion and concluding remarks

Our findings suggest that the Praesepe might be more metal-rich than the Hyades. To get deeper insights into this, we analysed -in the very same way- the HARPS-N spectrum of the Hyades member HD 28099, which we observed on August 2019 as part of our SPA program (the complete sample will be published in a forthcoming paper). The star is included in the high-resolution spectral analysis of Hyades solar analogues by Liu et al. (2016), who found  $T_{\text{eff}} = 5795 \pm 24 \text{ K}$ ,  $\log g = 4.47 \pm 0.04$  dex,  $\xi = 1.22 \pm 0.03 \text{ km s}^{-1}$ , and  $[\text{Fe}/\text{H}] = +0.154 \pm 0.016$  dex. We found an excellent agreement with that study, by obtaining:  $T_{\text{eff}} = 5800 \pm 70 \text{ K}$ ,  $\log g = 4.48 \pm 0.07$  dex,  $\xi = 1.02 \pm 0.13 \text{ km s}^{-1}$ , and  $[\text{Fe}/\text{H}] = +0.16 \pm 0.01$  dex. This results points out that no major systematic uncertainties plague our abundance analysis. Crucially, there is a difference in the iron content between Praesepe and the Hyades solar-type member HD 28099 of  $+0.05 \pm 0.01$  dex, which rules out a common origin and reconcile the gyro-chronological age with the isochrones, suggesting an age of  $\approx 570\text{--}600$  Myr, instead of  $700\text{--}750$  Myr. These relatively small differences in the chemical composition can emerge only when very accurate and strictly (line-by-line) differential abundances analysis are performed, as first shown in the work by Meléndez et al. (2014).

In Fig. 5 we plot metallicity as a function of the age for a sample of OCs from the quite homogeneous study by Ne-topil et al. (2016), considering only clusters in the solar surroundings ( $7.5 < R_{\text{GC}} < 9$  kpc). The very old OC NGC 6791 stands out in this distribution, but it is probably the oldest cluster known (age  $\approx 8$  Gyr, e.g., Brogaard et al. 2012) so for the dis-

**Table 5.** Stellar parameters and iron abundances from the HARPS-N optical spectra. The two errors reported for  $[\text{Fe}/\text{H}]_{\text{I}}$  and  $[\text{Fe}/\text{H}]_{\text{II}}$  represent uncertainties related to EW measurements and stellar parameters, respectively.

star	$T_{\text{eff}}(JK)$ (K)	$T_{\text{eff}}(VK)$ (K)	$T_{\text{eff}}^{\text{Phot}}(\text{K})$ (K)	$T_{\text{eff}}^{\text{Spec}}(\text{K})$ (K)	$\log g$ (dex)	$\xi$ ( $\text{km s}^{-1}$ )	$[\text{Fe}/\text{H}]_{\text{I}}$ (dex)	$[\text{Fe}/\text{H}]_{\text{II}}$ (dex)
N2632-6	5757	5908	5833	5870±80	4.45±0.15	1.00±0.15	0.20±0.01±0.08	0.20±0.03±0.08
N2632-7	5851	5954	5903	5950±80	4.55±0.15	1.15±0.15	0.23±0.01±0.07	0.22±0.04±0.08
N2632-8	6000	5954	5977	5977±75	4.55±0.15	1.30±0.20	0.27±0.01±0.07	0.23±0.03±0.08
N2632-9	5851	5951	5901	5920±80	4.50±0.15	1.35±0.18	0.21±0.02±0.07	0.18±0.05±0.08
N2632-10	5986	5989	5988	5968±80	4.58±0.15	1.20±0.20	0.22±0.01±0.07	0.19±0.03±0.08
N2632-25	5986	6146	6066	6150±70	4.55±0.17	1.35±0.20	0.20±0.01±0.07	0.21±0.03±0.09
N2632-26	5939	6149	6044	6044±73	4.50±0.17	1.18±0.20	0.18±0.01±0.07	0.22±0.03±0.09
N2632-27	5856	6089	5973	6000±80	4.50±0.17	1.30±0.18	0.20±0.01±0.07	0.17±0.04±0.09
N2632-28	5735	5668	5702	5600±70	4.48±0.14	1.00±0.20	0.20±0.01±0.07	0.19±0.03±0.08
N2632-32	5392	5475	5434	5475±100	4.50±0.13	1.00±0.20	0.20±0.02±0.08	0.18±0.05±0.08

**Table 6.** Abundances for light,  $\alpha$ -elements and Ni from the HARPS-N optical spectra.

star	$[\text{Na}/\text{Fe}]_{\text{NLTE}}$ (dex)	$[\text{Mg}/\text{Fe}]$ (dex)	$[\text{Al}/\text{Fe}]$ (dex)	$[\text{Si}/\text{Fe}]$ (dex)	$[\text{Ca}/\text{Fe}]$ (dex)	$[\text{Ti}/\text{Fe}]_{\text{I}}$ (dex)	$[\text{Ti}/\text{Fe}]_{\text{II}}$ (dex)	$[\text{Ni}/\text{Fe}]$ (dex)
N2632-6	-0.01±0.01	-0.02±0.04	0.03±0.06	0.00±0.03	0.03±0.04	0.00±0.03	-0.03±0.03	-0.03±0.02
N2632-7	0.04±0.02	-0.06±0.03	-0.05±0.03	-0.02±0.04	0.03±0.04	0.01±0.02	-0.02±0.03	-0.02±0.02
N2632-8	-0.04±0.04	-0.03±0.03	-0.02±0.01	-0.02±0.02	0.02±0.04	0.01±0.02	-0.02±0.03	0.00±0.03
N2632-9	0.03±0.04	-0.05±0.03	0.01±0.02	-0.01±0.03	0.02±0.04	0.04±0.02	0.04±0.03	-0.01±0.03
N2632-10	0.02±0.02	-0.08±0.03	0.00±0.04	-0.02±0.03	-0.01±0.04	0.06±0.03	0.04±0.03	-0.03±0.03
N2632-25	0.05±0.02	0.08±0.08	0.06±0.10	0.00±0.03	0.05±0.03	0.02±0.02	0.04±0.04	-0.01±0.02
N2632-26	-0.04±0.03	-0.01±0.05	0.04±0.03	0.00±0.02	0.04±0.04	-0.03±0.02	-0.01±0.03	-0.03±0.02
N2632-27	0.03±0.05	0.01±0.10	0.00±0.05	-0.04±0.02	0.05±0.04	-0.04±0.03	-0.01±0.03	-0.03±0.03
N2632-28	0.02±0.07	0.07±0.10	0.09±0.03	0.00±0.02	0.08±0.04	0.05±0.02	0.04±0.03	-0.01±0.02
N2632-32	0.05±0.03	0.04±0.08	0.09±0.06	-0.01±0.04	0.07±0.04	0.06±0.03	0.03±0.02	-0.01±0.03
Cluster ave.	+0.02±0.01	0.00±0.02	+0.03±0.02	-0.01±0.01	+0.04±0.01	+0.02±0.01	0.00±0.01	-0.02±0.01

cussion in our framework of young OCs is not relevant. For the Hyades, which is a critical comparison system here, we adopted the accurate value published by Liu et al. (2016), that is  $[\text{Fe}/\text{H}]=+0.16\pm0.01$  (this is because their analysis is strictly differential and includes only solar-type stars). Thus, there is a difference of  $+0.05\pm0.01$  between the iron content of Praesepe and Hyades. The value reported by Netopil et al. (2016), which is originally from Heiter et al. (2014), is  $[\text{Fe}/\text{H}]=+0.13\pm0.05$  (the metallicity is lower, but with larger error-bar). The plot clearly demonstrates that there are no significant above-solar clusters with ages younger than 1 Gyr, with *the Praesepe being the most metal-rich, young OC in the solar neighbourhood*. The possibility of a migration from an inner region of the Galactic disc seems intriguing. By adopting a  $[\text{Fe}/\text{H}]=+0.15$  dex, Quillen et al. (2018) estimated that, given its age and the current Galactocentric distance of  $R_{GC}=7.7$  Kpc, Praesepe might have formed at  $R_{GC}=5.9$  kpc and then migrated for  $d=1.8$  kpc at its current location (migration rate of  $2.7$  kpc  $\text{Gyr}^{-1}$ ). We may consider these values as lower limits, since our findings suggest a slightly more metal-rich content for this cluster.

Finally, the K2 mission detected five planets in the Hyades (3 planet-host stars, of which K2-136 with three planets; Mann et al. 2016, Livingston et al. 2018, Ciardi et al. 2018) and eight planets (with one planetary candidate, EPIC 211901114 b) in Praesepe (Obermeier et al. 2016; Mann et al. 2017; Pepper et al. 2017; Rizzuto et al. 2018; Livingston et al. 2019). As for radial velocities survey, ten additional planets have been discovered in four open clusters, of which three in the Praesepe cluster (Quinn et al. 2012; Malavolta et al. 2016). We might speculate

that this OC exhibits a quite large frequency of planets, in agreement with its relatively high metallicity, although a statistical study would be needed to confirm this clue. Moreover different planetary-search campaigns are heterogeneous in terms of sample selection and scientific drivers (very different planet masses, radii, and compositions are investigated) so that it is not straightforward to draw significant conclusions on this possible indication.

**Acknowledgements.** This work exploits the Simbad, VizieR, and NASA-ADS databases. This publication makes use of data products from the Two Micron All Sky Survey, which is a joint project of the University of Massachusetts and the Infrared Processing and Analysis Center/California Institute of Technology, funded by the National Aeronautics and Space Administration and the National Science Foundation. We warmly thank the GAPS team for sharing the solar spectrum acquired with GIARPS, and the TNG personnel for help during the observations. VD thanks V. Nascimbeni and R. Gratton for very useful discussions. The authors thank the anonymous referee for very helpful comments and suggestions.

## References

- An, D., Terndrup, D. M., Pinsonneault, M. H., et al. 2007, *ApJ*, 655, 233  
 Asplund, M., Grevesse, N., Sauval, A. J., & Scott, P. 2009, *ARA&A*, 47, 481  
 Boesgaard, A. M., Roper, B. W., & Lum, M. G. 2013, *ApJ*, 775, 58  
 Brandt, T. D. & Huang, C. X. 2015, *ApJ*, 807, 58  
 Brogaard, K., VandenBerg, D. A., Bruntt, H., et al. 2012, *A&A*, 543, A106  
 Caffau, E., Bonifacio, P., Oliva, E., et al. 2019, *A&A*, 622, A68  
 Cantat-Gaudin, T., Jordi, C., Vallenari, A., et al. 2018, *A&A*, 618, A93  
 Cardelli, J. A., Clayton, G. C., & Mathis, J. S. 1989, *ApJ*, 345, 245  
 Casagrande, L., Ramírez, I., Meléndez, J., Bessell, M., & Asplund, M. 2010, *A&A*, 512, A54



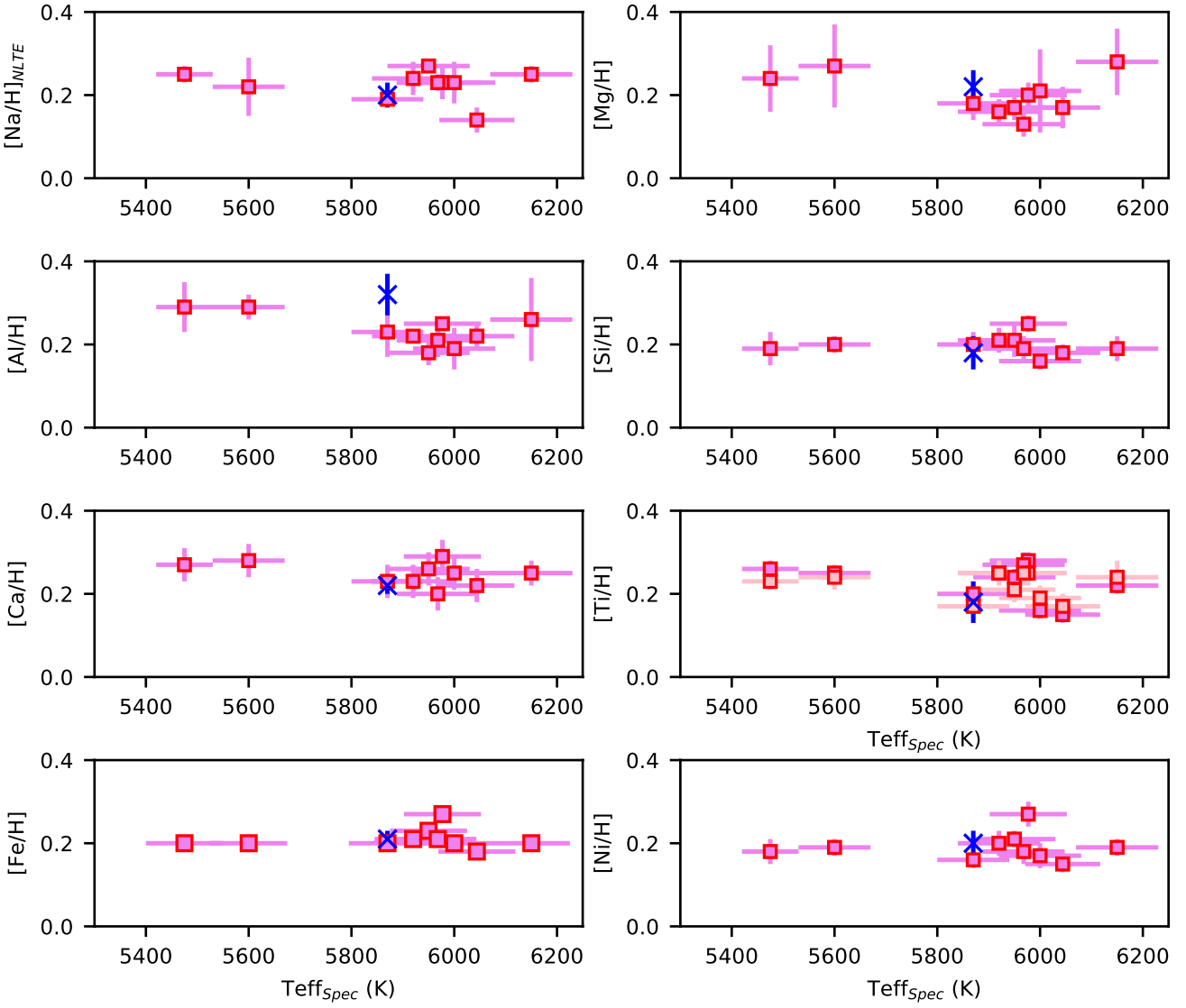


**Fig. 4.** Run of  $[X/H]$  ratios with spectroscopic effective temperatures for light (Na, Al),  $\alpha$ -elements (Mg, Si, Ca, and Ti), Fe and Ni from the HARPS-N spectra (squared symbols). GIANO-B results for star N2632-6 are labelled as (blue) cross sign. Error bars include uncertainties due to EW measurements. Ti II is labelled as small, light-pink symbols

- Castelli, F. & Kurucz, R. L. 2004, ArXiv Astrophysics e-prints [astro-ph/0405087]
- Chiappini, C., Romano, D., & Matteucci, F. 2003, MNRAS, 339, 63
- Ciardi, D. R., Crossfield, I. J. M., Feinstein, A. D., et al. 2018, AJ, 155, 10
- Claudi, R., Benatti, S., Carleo, I., et al. 2016, in Society of Photo-Optical Instrumentation Engineers (SPIE) Conference Series, Vol. 9908, Proc. SPIE, 99081A
- Cosentino, R., Lovis, C., Pepe, F., et al. 2014, in Society of Photo-Optical Instrumentation Engineers (SPIE) Conference Series, Vol. 9147, Proc. SPIE, 91478C
- Covino, E., Esposito, M., Barbieri, M., et al. 2013, A&A, 554, A28
- Cummings, J. D., Deliyannis, C. P., Maderak, R. M., & Steinhauer, A. 2017, AJ, 153, 128
- Delgado Mena, E., Lovis, C., Santos, N. C., et al. 2018, A&A, 619, A2
- Delorme, P., Collier Cameron, A., Hebb, L., et al. 2011, MNRAS, 413, 2218
- Donor, J., Frinchaboy, P. M., Cunha, K., et al. 2018, AJ, 156, 142
- D'Orazi, V., Biazzo, K., & Randich, S. 2011, A&A, 526, A103
- D'Orazi, V., Desidera, S., Gratton, R. G., et al. 2017, A&A, 598, A19
- Drazdauskas, A., Tautvaišienė, G., Randich, S., et al. 2016, A&A, 589, A50
- Edvardsson, B., Andersen, J., Gustafsson, B., et al. 1993, A&A, 500, 391
- Evans, D. W., Riello, M., De Angeli, F., et al. 2018, A&A, 616, A4
- Frasca, A., Alonso-Santiago, J., Catanzaro, G., et al. 2019, arXiv e-prints, arXiv:1910.02006
- Friel, E. D. & Boesgaard, A. M. 1992, ApJ, 387, 170
- Fujii, M. S. & Hori, Y. 2019, A&A, 624, A110
- Gilmore, G., Randich, S., Asplund, M., et al. 2012, The Messenger, 147, 25
- Gossage, S., Conroy, C., Dotter, A., et al. 2018, ApJ, 863, 67
- Heiter, U., Soubiran, C., Netopil, M., & Paurzen, E. 2014, A&A, 561, A93
- Johnson, J. A., Aller, K. M., Howard, A. W., & Crepp, J. R. 2010, PASP, 122, 905
- Lawler, J. E., Guzman, A., Wood, M. P., Sneden, C., & Cowan, J. J. 2013, ApJS, 205, 11
- Lind, K., Asplund, M., Barklem, P. S., & Belyaev, A. K. 2011, A&A, 528, A103
- Liu, F., Yong, D., Asplund, M., Ramírez, I., & Meléndez, J. 2016, MNRAS, 457, 3934
- Livingston, J. H., Dai, F., Hirano, T., et al. 2018, AJ, 155, 115
- Livingston, J. H., Dai, F., Hirano, T., et al. 2019, MNRAS, 484, 8
- Magrini, L., Randich, S., Kordopatis, G., et al. 2017, A&A, 603, A2
- Malavolta, L., Nascimbeni, V., Piotto, G., et al. 2016, A&A, 588, A118
- Mann, A. W., Gaidos, E., Mace, G. N., et al. 2016, ApJ, 818, 46
- Mann, A. W., Gaidos, E., Vanderburg, A., et al. 2017, AJ, 153, 64
- Martín, E. L., Lodieu, N., Pavlenko, Y., & Béjar, V. J. S. 2018, ApJ, 856, 40
- Meléndez, J., Ramírez, I., Karakas, A. I., et al. 2014, ApJ, 791, 14
- Minchev, I., Chiappini, C., & Martig, M. 2013, A&A, 558, A9
- Netopil, M., Paurzen, E., Heiter, U., & Soubiran, C. 2016, A&A, 585, A150
- Obermeier, C., Henning, T., Schlieder, J. E., et al. 2016, AJ, 152, 223
- Oliva, E., Biliotti, V., Baffa, C., et al. 2012a, in Society of Photo-Optical Instrumentation Engineers (SPIE) Conference Series, Vol. 8453, Proc. SPIE, 84532T

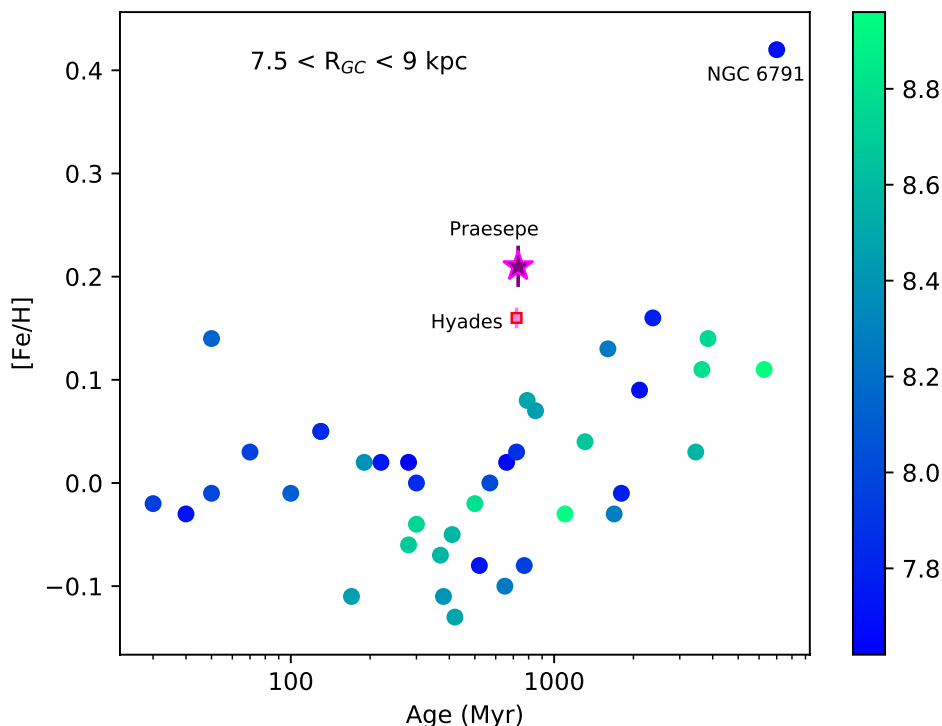


**Fig. 5.**  $[\text{Fe}/\text{H}]$  as a function of age for OCs in the solar neighbourhood. Data for ages, metallicity and  $R_{\text{GC}}$  are from Netopil et al. (2016) for all OCs, with the exception of the Hyades ( $[\text{Fe}/\text{H}]$  from Liu et al. 2016). OCs from Netopil et al. have been colour-coded according to the Galactocentric radius ( $R_{\text{GC}}$ )

- Oliva, E., Origlia, L., Maiolino, R., et al. 2012b, in Society of Photo-Optical Instrumentation Engineers (SPIE) Conference Series, Vol. 8446, Proc. SPIE, 84463T
- Origlia, L., Dalessandro, E., Sanna, N., et al. 2019, arXiv e-prints, arXiv:1908.07779
- Origlia, L., Oliva, E., Baffa, C., et al. 2014, in Society of Photo-Optical Instrumentation Engineers (SPIE) Conference Series, Vol. 9147, Proc. SPIE, 91471E
- Pace, G., Pasquini, L., & François, P. 2008, A&A, 489, 403
- Pepper, J., Gillen, E., Parviainen, H., et al. 2017, AJ, 153, 177
- Quillen, A. C., Nolting, E., Minchev, I., De Silva, G., & Chiappini, C. 2018, MNRAS, 475, 4450
- Quinn, S. N., White, R. J., Latham, D. W., et al. 2012, ApJ, 756, L33
- Rainer, M., Harutyunyan, A., Carleo, I., et al. 2018, in Society of Photo-Optical Instrumentation Engineers (SPIE) Conference Series, Vol. 10702, Ground-based and Airborne Instrumentation for Astronomy VII, 1070266
- Reddy, A. B. S., Lambert, D. L., & Giridhar, S. 2016, MNRAS, 463, 4366
- Rizzuto, A. C., Vanderburg, A., Mann, A. W., et al. 2018, AJ, 156, 195
- Ruffoni, M. P., Allende Prieto, C., Nave, G., & Pickering, J. C. 2013, ApJ, 779, 17
- Ruffoni, M. P., Den Hartog, E. A., Lawler, J. E., et al. 2014, MNRAS, 441, 3127
- Santos, N. C., Israelian, G., & Mayor, M. 2004, A&A, 415, 1153
- Skrutskie, M. F., Cutri, R. M., Stiening, R., et al. 2006, AJ, 131, 1163
- Snedden, C. A. 1973, PhD thesis, THE UNIVERSITY OF TEXAS AT AUSTIN.
- Sousa, S. G., Santos, N. C., Israelian, G., Mayor, M., & Monteiro, M. J. P. F. G. 2007, A&A, 469, 783
- Spina, L., Randich, S., Magrini, L., et al. 2017, A&A, 601, A70
- Taylor, B. J. 2006, AJ, 132, 2453
- Viana Almeida, P., Santos, N. C., Melo, C., et al. 2009, A&A, 501, 965



## Appendix A: Linelists

The complete line list exploited to calculate synthetic NIR spectra is shown in Table A.1: wavelengths, species, excitation potential (EP), and  $\log gf$  of the spectral lines are given in Columns 1,2,3, and 4 respectively. Abundances for star N2632-6 are given in Column 5, while the solar value obtained from our analysis is reported in Column 6. References for  $\log gf$  include Ruffoni et al. (2013), when available, and Kurucz and NIST databases. The latter were adjusted to the solar abundances as needed (note that our stars are very similar to the Sun in terms of stellar parameters ( $T_{\text{eff}}$ , and  $\log g$ ), so our choice can be considered fairly safe).

The line list for the optical HARPS-N spectra is displayed in Table A.2. The analysis has been carried out via EW measurements. The source of oscillator strengths include the NIST database, Lawler et al. (2013) for Ti lines, linelists published by D'Orazi et al. (2017), and Ruffoni et al. (2014) for Fe I.

**Table A.1.** Line-by-line abundances and atomic parameters for GIANO-B spectra of star N2632-6 (spectral synthesis analysis).

Wavelength (Å)	Ion	E.P. (eV)	$\log gf$	A(X)	A(X) <sub>⊙</sub>
12679.144	11.0	3.614	−0.04	6.44	6.24
9986.474	12.0	5.927	−1.52	7.75	7.60
9993.210	12.0	5.928	−1.30	7.80	7.60
12039.861	12.0	5.749	−1.45	7.70	7.60
12417.912	12.0	5.927	−1.66	7.90	7.55
12422.996	12.0	5.927	−1.18	7.90	7.63
15886.18	12.0	5.941	−2.13	7.85	7.58
16750.564	13.0	4.084	0.41	6.80	6.45
16763.360	13.0	4.084	−0.55	6.75	6.45
12103.535	14.0	4.926	−0.29	7.70	7.66
12270.692	14.0	4.950	−0.41	7.70	7.55
16060.009	14.0	5.949	−0.44	7.81	7.51
16094.787	14.0	5.959	0.31	7.61	7.51
10838.970	20.0	4.874	−0.03	6.58	6.34
12909.07	20.0	4.427	−0.43	6.50	6.30
10396.80	22.0	0.848	−1.43	5.05	4.95
15543.75	22.0	1.878	−1.27	5.15	4.90
15051.749	26.0	5.348	0.26	7.90	7.35
15207.526	26.0	5.381	0.40	7.65	7.50
15294.562	26.0	5.304	0.88	7.60	7.52
15591.497	26.0	6.237	0.90	7.68	7.50
15604.223	26.0	6.237	0.61	7.55	7.48
15621.654	26.0	5.535	0.77	7.60	7.50
15648.510	26.0	5.422	−0.51	7.55	7.50
15816.633	26.0	5.951	−0.43	7.60	7.50
15822.817	26.0	5.638	0.30	7.65	7.50
15835.167	26.0	6.298	0.95	7.60	7.50
16153.247	26.0	5.348	−0.66	7.80	7.55
16165.032	26.0	6.314	0.89	7.83	7.50
16174.978	26.0	6.375	−0.26	7.82	7.50
16179.585	26.0	6.314	0.14	7.77	7.45
16195.063	26.0	6.389	−0.05	7.68	7.48
16394.392	26.0	5.951	0.22	7.75	7.50
16398.170	26.0	5.916	0.17	7.75	7.50
16506.296	26.0	5.942	−0.47	7.68	7.50
16517.226	26.0	6.282	0.65	7.90	7.50
15199.658	28.0	5.465	−0.64	6.45	6.26
16310.504	28.0	5.278	0.07	6.42	6.22

**Table A.2.** Linelist for the HARPS-N spectra.

Wavelength (Å)	Ion	E.P. (eV)	log $gf$
6154.23	11.0	2.1	-1.57
6160.75	11.0	2.1	-1.25
4730.03	12.0	4.3	-2.30
5711.09	12.0	4.3	-1.71
6696.02	13.0	3.1	-1.62
6698.67	13.0	3.1	-1.92
5645.61	14.0	4.9	-2.04
5665.56	14.0	4.9	-1.94
5684.48	14.0	4.9	-1.55
5690.42	14.0	4.9	-1.74
6125.02	14.0	5.6	-1.52
6142.48	14.0	5.6	-1.50
6155.13	14.0	5.6	-0.72
6237.32	14.0	5.6	-1.05
6243.81	14.0	5.6	-1.29
6244.47	14.0	5.6	-1.32
6721.84	14.0	5.8	-1.13
5260.39	20.0	2.5	-1.78
5261.70	20.0	2.5	-0.58
5581.96	20.0	2.5	-0.67
5857.45	20.0	2.9	0.26
5867.56	20.0	2.9	-1.60
6169.56	20.0	2.5	-0.52
6455.60	20.0	2.5	-1.35
6499.65	20.0	2.5	-0.81
6508.85	20.0	2.5	-2.53
4186.12	22.0	1.5	-0.24
4287.40	22.0	0.8	-0.37
4427.10	22.0	1.5	0.23
4453.31	22.0	1.4	-0.03
4453.70	22.0	1.8	0.10
4471.24	22.0	1.7	-0.15
4518.02	22.0	0.8	-0.25
4548.76	22.0	0.8	-0.28
4623.10	22.0	1.7	0.16
4722.61	22.0	1.0	-1.47
4758.90	22.0	0.8	-2.17
4778.25	22.0	2.2	-0.35
4781.71	22.0	0.8	-1.95
4797.98	22.0	2.3	-0.63
4805.41	22.0	2.3	0.07
4820.41	22.0	1.5	-0.38
4840.87	22.0	0.8	-0.43
4870.12	22.0	2.2	0.44
4885.08	22.0	1.8	0.41
4899.91	22.0	1.8	0.31
4937.73	22.0	0.8	-2.08
4995.07	22.0	2.2	-1.00
5016.16	22.0	0.8	-0.48
5020.03	22.0	0.8	-0.33
5036.46	22.0	1.4	0.14
5038.40	22.0	1.4	0.02
5040.61	22.0	0.8	-1.67
5043.58	22.0	0.8	-1.59
5062.10	22.0	2.1	-0.39
5064.65	22.0	0.0	-0.94
5087.06	22.0	1.4	-0.88
5145.46	22.0	1.4	-0.54
5192.97	22.0	0.0	-0.95

Table A.2. Continued.

Wavelength (Å)	Ion	EP (eV)	log gf
5210.38	22.0	0.0	−0.82
5219.70	22.0	0.0	−2.22
5295.78	22.0	1.0	−1.59
5389.17	22.0	0.8	−2.35
5471.19	22.0	1.4	−1.42
5503.90	22.0	2.5	−0.05
5514.34	22.0	1.4	−0.66
5514.53	22.0	1.4	−0.50
5565.47	22.0	2.2	−0.22
5739.98	22.0	2.2	−0.92
5866.45	22.0	1.0	−0.79
5880.27	22.0	1.0	−2.00
5922.11	22.0	1.0	−1.38
5937.81	22.0	1.0	−1.94
6258.10	22.0	1.4	−0.39
6261.10	22.0	1.4	−0.53
6303.76	22.0	1.4	−1.58
6312.24	22.0	1.4	−1.55
6554.22	22.0	1.4	−1.15
4316.79	22.1	2.0	−1.62
4320.95	22.1	1.1	−1.88
4395.83	22.1	1.2	−1.93
4443.80	22.1	1.0	−0.71
4468.49	22.1	1.1	−0.63
4493.52	22.1	1.0	−2.78
4518.33	22.1	1.0	−2.56
4571.97	22.1	1.5	−0.31
4583.40	22.1	1.1	−2.84
4609.26	22.1	1.1	−3.32
4657.20	22.1	1.2	−2.29
4708.66	22.1	1.2	−2.35
4764.52	22.1	1.2	−2.69
4798.53	22.1	1.0	−2.66
4865.61	22.1	1.1	−2.70
4874.00	22.1	3.0	−0.86
4911.19	22.1	3.1	−0.64
5069.09	22.1	3.1	−1.62
5185.90	22.1	1.8	−1.41
5211.53	22.1	2.5	−1.41
5336.78	22.1	1.5	−1.60
5381.02	22.1	1.5	−1.97
5396.24	22.1	1.5	−3.18
5418.76	22.1	1.5	−2.13
6680.13	22.1	3.0	−1.89
4007.27	26.0	2.7	−1.66
4010.18	26.0	3.6	−2.03
4014.27	26.0	3.0	−2.33
4080.88	26.0	3.6	−1.54
4423.84	26.0	3.6	−1.61
4547.85	26.0	3.5	−1.01
4587.13	26.0	3.5	−1.74
4602.00	26.0	1.6	−3.15
4630.12	26.0	2.2	−2.59
4635.85	26.0	2.8	−2.36
4690.14	26.0	3.6	−1.64
4704.95	26.0	3.6	−1.57
4733.59	26.0	1.4	−2.99
4745.80	26.0	3.6	−1.27
4779.44	26.0	3.4	−2.02
4787.83	26.0	2.9	−2.60

Table A.2. Continued.

Wavelength (Å)	Ion	EP (eV)	log gf
4788.76	26.0	3.2	-1.76
4799.41	26.0	3.6	-2.23
4802.88	26.0	3.6	-1.51
4807.71	26.0	3.3	-2.15
4808.15	26.0	3.2	-2.79
4809.94	26.0	3.5	-2.72
4835.87	26.0	4.1	-1.50
4839.54	26.0	3.2	-1.82
4844.01	26.0	3.5	-2.05
4875.88	26.0	3.3	-2.02
4882.14	26.0	3.4	-1.64
4892.86	26.0	4.2	-1.29
4907.73	26.0	3.4	-1.84
4918.01	26.0	4.2	-1.36
4946.39	26.0	3.3	-1.17
4950.10	26.0	3.4	-1.49
4994.13	26.0	0.9	-3.05
5198.71	26.0	2.2	-2.13
5225.53	26.0	0.1	-4.78
5247.05	26.0	0.0	-4.94
5250.21	26.0	0.1	-4.93
5295.31	26.0	4.4	-1.59
5373.71	26.0	4.4	-0.71
5379.57	26.0	3.6	-1.51
5386.33	26.0	4.1	-1.67
5441.34	26.0	4.3	-1.63
5466.40	26.0	4.3	-0.63
5466.99	26.0	3.5	-2.23
5491.83	26.0	4.1	-2.18
5554.89	26.0	4.5	-0.27
5560.21	26.0	4.4	-1.09
5618.63	26.0	4.2	-1.25
5638.26	26.0	4.2	-0.72
5651.47	26.0	4.4	-1.90
5679.02	26.0	4.6	-0.82
5705.46	26.0	4.3	-1.35
5731.76	26.0	4.2	-1.20
5852.22	26.0	4.5	-1.23
5855.08	26.0	4.6	-1.47
5956.69	26.0	0.8	-4.59
5987.07	26.0	4.8	-0.42
6005.54	26.0	2.5	-3.60
6065.48	26.0	2.6	-1.52
6079.01	26.0	4.6	-1.02
6082.71	26.0	2.2	-3.57
6093.64	26.0	4.6	-1.40
6096.67	26.0	3.9	-1.83
6151.62	26.0	2.1	-3.29
6165.36	26.0	4.1	-1.47
6173.34	26.0	2.2	-2.88
6187.99	26.0	3.9	-1.62
6200.31	26.0	2.6	-2.43
6213.43	26.0	2.2	-2.48
6219.28	26.0	2.2	-2.43
6226.74	26.0	3.8	-2.12
6232.64	26.0	3.6	-1.23
6380.74	26.0	4.1	-1.37
6430.85	26.0	2.1	-2.00
6593.87	26.0	2.4	-2.42
6597.56	26.0	4.8	-0.97

**Table A.2.** Continued.

Wavelength (Å)	Ion	EP (eV)	log gf
6625.02	26.0	1.0	−5.33
6703.57	26.0	2.7	−3.06
6705.10	26.0	4.6	−0.87
6710.32	26.0	1.4	−4.76
6713.75	26.0	4.8	−1.50
6725.36	26.0	4.1	−2.10
6726.67	26.0	4.6	−1.13
6739.52	26.0	1.5	−4.79
6750.15	26.0	2.4	−2.61
6793.26	26.0	4.0	−2.32
4508.29	26.1	2.8	−2.35
4576.34	26.1	2.8	−2.98
4582.83	26.1	2.8	−3.22
4620.52	26.1	2.8	−3.31
4629.34	26.1	2.8	−2.48
4635.32	26.1	5.9	−1.58
4670.18	26.1	2.5	−4.07
4993.35	26.1	2.8	−3.68
5234.62	26.1	3.2	−2.18
5264.80	26.1	3.2	−3.13
5414.07	26.1	3.2	−3.58
6084.09	26.1	3.1	−3.88
6149.24	26.1	3.8	−2.84
6247.55	26.1	3.8	−2.43
6369.46	26.1	2.8	−4.11
6432.68	26.1	2.8	−3.57
6456.38	26.1	3.9	−2.18
4904.41	28.0	3.5	−0.25
4953.20	28.0	3.7	−0.68
4998.22	28.0	3.6	−0.79
5084.09	28.0	3.6	−0.07
5088.53	28.0	3.8	−1.06
5115.39	28.0	3.8	−0.13
5593.73	28.0	3.9	−0.77
5748.35	28.0	1.6	−3.24
5846.99	28.0	1.6	−3.45
5996.73	28.0	4.2	−1.06
6086.28	28.0	4.2	−0.45
6111.07	28.0	4.0	−0.83
6130.13	28.0	4.2	−0.89
6204.60	28.0	4.0	−1.15
6223.98	28.0	4.1	−0.97
6322.16	28.0	4.1	−1.21